Transitions of Morphological Patterns of Crystallizing Polycarbonate in Thin Films

Yuesheng Ye,[1,#] Bohyun Kim,[2,] Joonil Seog,[2,] Kyu Yong Choi[1,*]

[1]*Department of Chemical and Biomolecular Engineering, University of Maryland, College Park, Maryland 20742*
[2]*Department of Materials Science and Engineering and Fischell Department of Bioengineering, University of Maryland, College Park, Maryland 20742*

Received 4 April 2011; accepted 16 May 2011
DOI 10.1002/app.34920
Published online 5 October 2011 in Wiley Online Library (wileyonlinelibrary.com).

ABSTRACT: This article reports the transitions of morphological patterns of polycarbonate crystals in thin films by solvent-induced crystallization (SINC). As a substrate (silica glass) deposited with an amorphous and micron-thick bisphenol A polycarbonate polymer film is partially dipped into a liquid acetone bath, acetone penetrated rapidly through the polymer film. The rate of acetone penetration is significantly higher than the predicted by Fickian diffusion or anomalous diffusion model, indicating that the capillary force through stress-induced cracks may have played a major role in the upward transport of acetone through the polymer films. The morphologies of polycarbonate at different vertical positions on a substrate surface were analyzed by scanning electron microscopy and atomic force microscopy. It was observed that depending on the local acetone concentration the polymer morphologies showed quite diverse patterns ranging from stress-induced cracks to fully developed three-dimensional spherulites. The diverse morphologies developed during the thin film SINC may serve as a useful platform for further detailed mechanistic analysis of structures and crystallization kinetics. © 2011 Wiley Periodicals, Inc. J Appl Polym Sci 124: 560–567, 2012

Key words: bisphenol A polycarbonate; thin film; solvent-induced crystallization; spherulites; stress-induced crazing

INTRODUCTION

Amorphous bisphenol A (2,2-bis(4-hydroxyphenyl) propane) polycarbonate (BAPC) is widely used as optical materials for lenses, CDs, DVDs, and bottles. It can be crystallized by thermal annealing or solvent-induced crystallization (SINC) techniques. The thermal annealing is a very slow crystallization process (>100 h at 170–205°C) because of the rigidity of polymer backbone that hinders the rearrangement of the polymer molecules to an ordered crystalline structure.[1,2] BAPC can be rapidly crystallized by SINC using plasticizing solvents,[3] nuclear agents,[4] organic liquids,[5] organic vapors,[6] and super critical carbon dioxide.[7] The other methods such as the wet-drawn process[8] and high-pressure molding[9] are also often used to crystallize polycarbonates. In SINC technique, the molecular interactions between the penetrating molecules of a swelling agent and the polymer chain segments greatly reduce the glass transition temperature (T_g) of the polymer and significantly enhance chain mobility, relaxation, and rearrangement, leading to crystallization.[10]

Acetone is one of the most commonly used swelling agents used either in liquid or vapor form to induce crystallization of BAPC polymer.[10–16] Using liquid acetone and a 254-μm thick free-standing polycarbonate film, Wilkes and Parlapiano[13] crystallized polycarbonate to three-dimensional BAPC spherulites with fibrils growing on the top surface of the spherulites. A spherulitic structure of BAPC polymer with nanometer- and micrometer-sized protrusions on the surface of crystallized BAPC was also reported.[15] The morphological structures of BAPC polymers depend on the specific crystallization procedure and polymer properties such as molecular weight[12] and film thickness.[16] In most of the morphological studies on the crystalline BAPC, relatively thick free-standing films (254 μm,[13] 1200 μm[15]) were used. In our recent work,[16] polycarbonate films of 4–10 μm thickness crystallized to form a layer of micron-sized three-dimensional spherulitic particles when the amorphous polymer film was treated with a swelling agent (acetone). Such phenomenon can be observed only when the substrate-supported films within a certain range of film thickness were used. However, the crystallization occurred too fast to monitor the evolution of crystalline particle morphology.

In this study, we investigated how the spherulitic structures of crystallizing BAPC films evolved from

[#]*Present address:* 3141 Chestnut Street, Chemical and Biological Engineering Department, Drexel University, Pennsylvania 19104.
[*]*Correspondence to:* K.Y. Choi (choi@umd.edu).

an amorphous film to three-dimensional spherulites. A silica substrate coated with an amorphous BAPC film was vertically placed in an acetone bath. As acetone diffused through the BAPC thin film above the liquid level, the progression of the crystallization was monitored at different vertical positions from the liquid–air interface. This technique provides a quiescent growth environment which enables us to capture the full spectrum of morphological development of BAPC thin films. The morphological structures of the crystallizing polymer were analyzed by scanning electron microscopy (SEM) and atomic force microscopy (AFM).

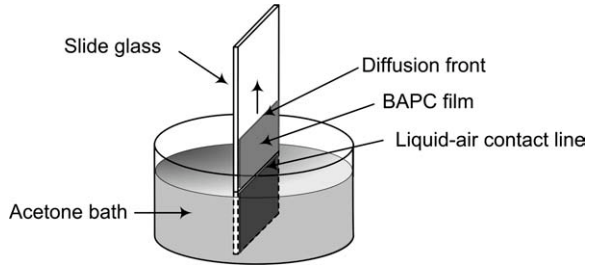

Figure 1 Schematic drawing of controlled solvent-induced crystallization of BAPC thin film in an acetone bath. Amorphous film with 5.5-μm thickness was immersed into acetone bath vertically. At 300 s of immersion time the diffusion front was moved to ~ 1 cm from liquid-air interface.

EXPERIMENTAL

Materials

The BAPC polymer sample ($\overline{M}_w = 8910$) used in this study was obtained from the melt transesterification of diphenyl carbonate and bisphenol A with LiOH H_2O as a catalyst.[17] HPLC-grade chloroform and acetone were used as received from Sigma-Aldrich (St. Louis, MO). Microscopic silica slide glasses ($25 \times 75 \times 1$ mm^3, Fisher) were used as substrates for the solution casting of polymer thin films.

Amorphous thin film preparation and controlled solvent-induced crystallization

Amorphous BAPC films on the silica slide glass were prepared by solution casting. BAPC polymer particles were first dissolved in chloroform to a desired polymer concentration (~ 12 wt %) at ambient temperature. A clean and dried slide glass was immersed in the polymer solution for about 1–2 s, and then removed from the solution bath. One side of a film was removed by a razor blade and the other side film was air and vacuum dried to a ~ 5.5-μm thick amorphous and transparent film. The film thickness was measured by a Mitutoyo Micrometer (Kawasaki, Japan). To induce crystallization in the polymer film, the polymer coated slide glass was placed vertically in an acetone bath for 300 s (Fig. 1) at room temperature. As the slide glass was dipped into the acetone bath, the polymer film exposed to air became opaque, indicating the penetration of acetone into the polymer film and crystallization. After removed from the acetone bath, the film was first air dried and then vacuum dried in an oven at ambient temperature for 24 h.

Characterization of thin film morphology

The morphology of the crystallized BAPC film was investigated using Amory 1820-D and Hitachi SU-70 scanning electron microscope (SEM, Schaumburg, IL) operating at 20 kv and at 5 kv, respectively. Before the SEM analysis, polymer film samples were coated with Au–Pd in a Denton vacuum evaporator. The nanoscale structure of the crystallized BAPC films was also investigated by molecular force probe 3D, a variant of AFM (MFP-3D, Asylum Research, Santa Barbara, CA). The morphology of the film was obtained in a tapping mode at 0.5–1 Hz scan rate using silicon tip (Vistaprobes T180R, Nanoscience Instruments, Phoenix, AZ).

RESULTS AND DISCUSSION

When a slide glass with amorphous BAPC films on the surface was partially immersed in the acetone bath as shown in Figure 1, acetone quickly penetrated into the film above the liquid-air contact line, causing it to become opaque. The opaque film formation suggested that crystallization of BAPC occurred as acetone diffused into the thin film of BAPC. The diffusion front which is defined by the line between clear and opaque region moved at a speed of ~ 1 cm (from the liquid–air contact line) in 300 s before the movement stopped. It should be noted that the diffusion of acetone vapor in BAPC films is much lower than that of liquid acetone since under a low partial pressure of acetone vapor, it takes long time (on order of hours) to crystallize the BAPC film.[18] Thus, the speed of the diffusion front strongly suggests that the acetone liquid, not acetone vapor is primarily responsible for thin film crystallization.

Let us consider the diffusion behaviors of acetone in BAPC thin film. In general, the solvent transport in a glassy polymer can be classified into three categories: Case I (Fickian diffusion), Case II diffusion, and anomalous diffusion (the combination of Case I and Case II diffusion).[19] The Fickian diffusion is driven by the concentration gradient and Case II diffusive transport is controlled by the stress relaxation.

The diffusion of liquid acetone in BAPC polymer was treated as either Fickian diffusion[20,21] or anomalous diffusion.[22,23] For Fickian diffusion, the concentration profiles in the semi-infinite and homogeneous polymer film can be obtained by solving a dynamic diffusion equation and the solution is expressed by the following equation[24]

$$C = C_0 \mathrm{erfc}\left(\frac{x}{2\sqrt{Dt}}\right) \quad (1)$$

where erfc is the complementary error function and D, x, and C_0 are the solvent diffusivity, penetration distance, and the bulk phase solvent concentration, respectively. For the case of combined Fickian and Case II diffusion, the concentration profiles in the semi-infinite and homogeneous polymer film can be expressed as,[25]

$$C = \frac{C_0}{2}\left[\exp\left(\frac{xv}{D}\right)\mathrm{erfc}\left(\frac{x+vt}{2\sqrt{Dt}}\right) + \mathrm{erfc}\left(\frac{x-vt}{2\sqrt{Dt}}\right)\right] \quad (2)$$

where v is the velocity of solvent penetration as a direct consequence of the internal stress effect in the Case II transport. The diffusivity values of acetone reported in literature range from 3×10^{-7} to 1.26×10^{-6} cm^2/s.[20–23] The diffusivity is also affected by temperature and polymer molecular weight.[26] Figure 2 shows the acetone concentration profiles in the BAPC film at 300 s calculated using the Fickian diffusion model and the anomalous diffusion model with the parameters given in literature. Fickian diffusion model predicted the acetone penetration depth was only about 0.04–0.06 cm using two reported diffusivities during this time period. Turska[21] and Ouyang[27] experimentally showed that the penetration distance of acetone was about 0.03 cm at 300 s in a thick free-standing BAPC polymer film, which was quite consistent with the calculated results using eq. (1). The penetration distance estimated using the combined Fickian and Case II diffusion model [eq. (2)] was 0.08 cm during the same time period. However, in our study the observed penetration distance from the liquid-air contact line was $\sim$ 1 cm at 300 s, which was significantly larger than either calculated or experimentally measured values for thicker films reported in the literature.[13,15] This indicates that the acetone penetrates along the micron-thick film much faster than in the bulk of a thick BAPC film. The drastically enhanced diffusion of acetone in a micron-thick film used in this study indicates that the other mechanisms are operative in addition to the simple diffusion and stress relaxation mechanism. In addition, morphologies formed during SINC of thin BAPC films may be different from those in the bulk phase or thick films.

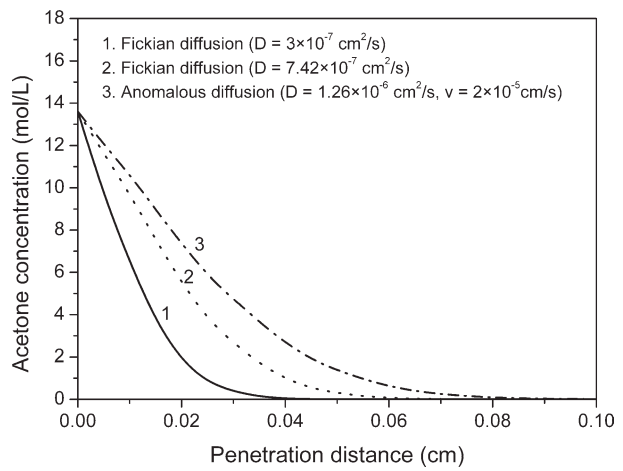

Figure 2 Acetone concentration profiles as a function of penetration distance calculated by Fickian diffusion model (Curves 1 and 2) and anomalous diffusion model (Curve 3) (dipping time = 300 s).

Figure 3 shows a series of SEM images of the BAPC thin film along the height (see Fig. 1) above the liquid-air contact line. These images clearly show how different morphological patterns evolved at different locations along the film due to the acetone concentration gradient. Above diffusion front, [Fig. 3(a)], amorphous BAPC film remained as unchanged. Figure 3(b) which is 1 cm below Figure 3(a) shows the appearance of a loose structure with the tip of a craze around the diffusion front. The local stress increase due to diffusion of the swelling agent is likely to be the cause of the craze formation.[28] However, the acetone concentration was not high enough to induce the formation of well-defined crystalline structures in this region. Figure 3(c–g) show that as the polymer film was exposed to higher acetone concentration, cracks, cavities, and voids structures developed. These micron-sized cracks and cavities developed in the entire thin film thickness, providing diffusion channels and facilitating the penetration of liquid acetone in the thin film through capillary force. The formation of these cracks and voids seem to explain the huge increase of penetration distance compared with the penetration distances calculated by the models [eqs. (1) and (2)]. As a result, factors such as film thickness that can affect the formation of cracks and voids may affect the penetration depth, and hence the morphology. The diffusion front barely moved after 300 s, indicating that gravity force prevented the further penetration of the acetone into thin films.

A closer look at the spherulitic morphologies of Figure 3(g) reveals two different types of morphological patterns: two-dimensional spherulites at the film surface and the three-dimensional spherulites below the film surface. When the acetone penetrated into the film through cracks created by stress

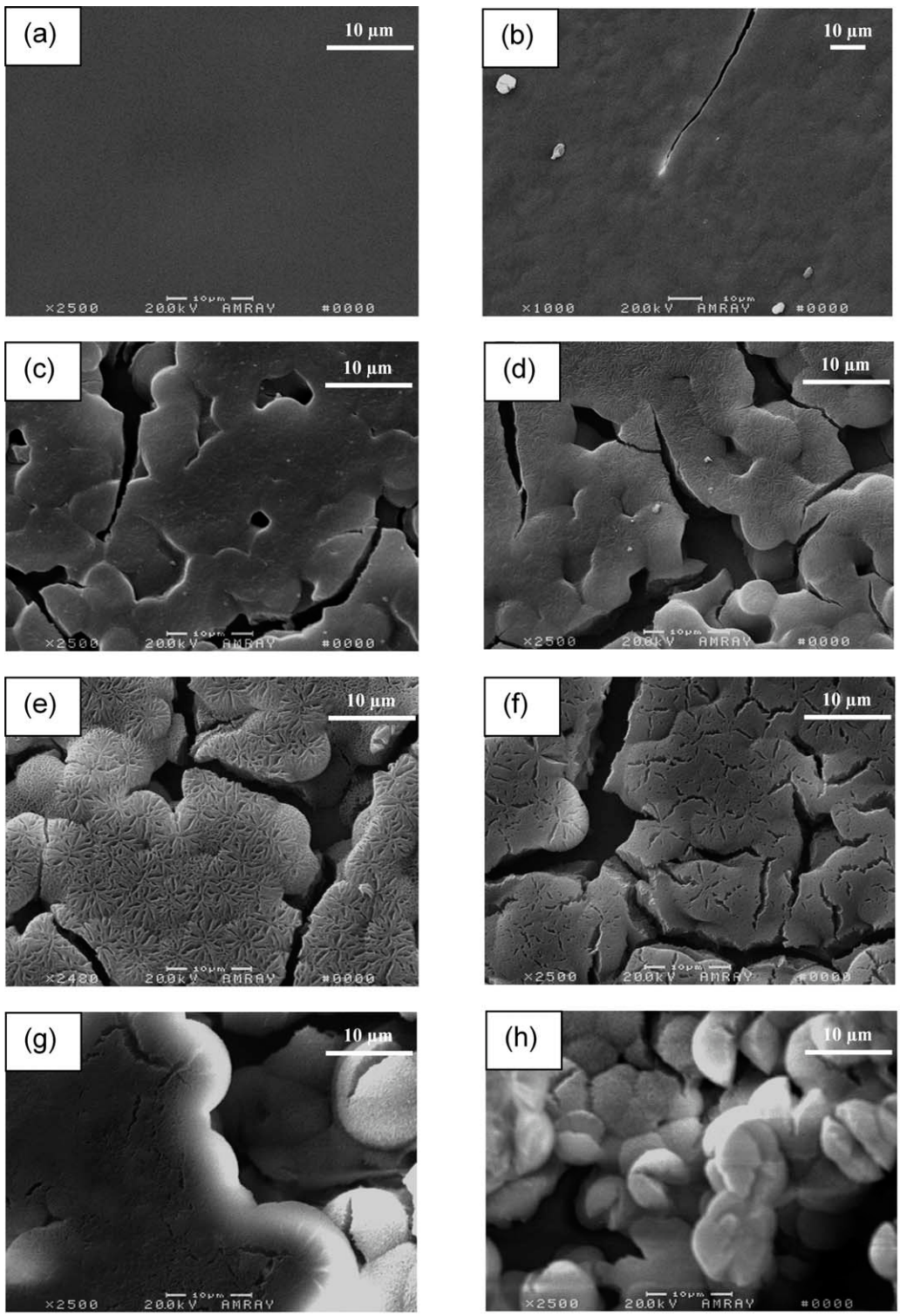

Figure 3 SEM images of morphology patterns above the contact line (a–h, from top to bottom, dipping time = 300 s), and the approximate distance away from the contact line: (a) 20 mm, (b) 10 mm, (c) 9 mm, (d) 8 mm, (e) 6 mm, (f) 4 mm, (g) 3 mm, and (h) 0.1 mm.

relaxation process, interior of the film was exposed to relatively high concentration to form three-dimensional spherulites. In contrast, the surface of the film might have experienced evaporation of acetone, which did not provide sufficiently high "solvent power" to complete the formation of three-dimensional spherulites. At the position right above the contact line [Fig. 3(h)], the amorphous film was completely transformed into three-dimensional spherulitic structures of 5–10 μm in diameter. The complete

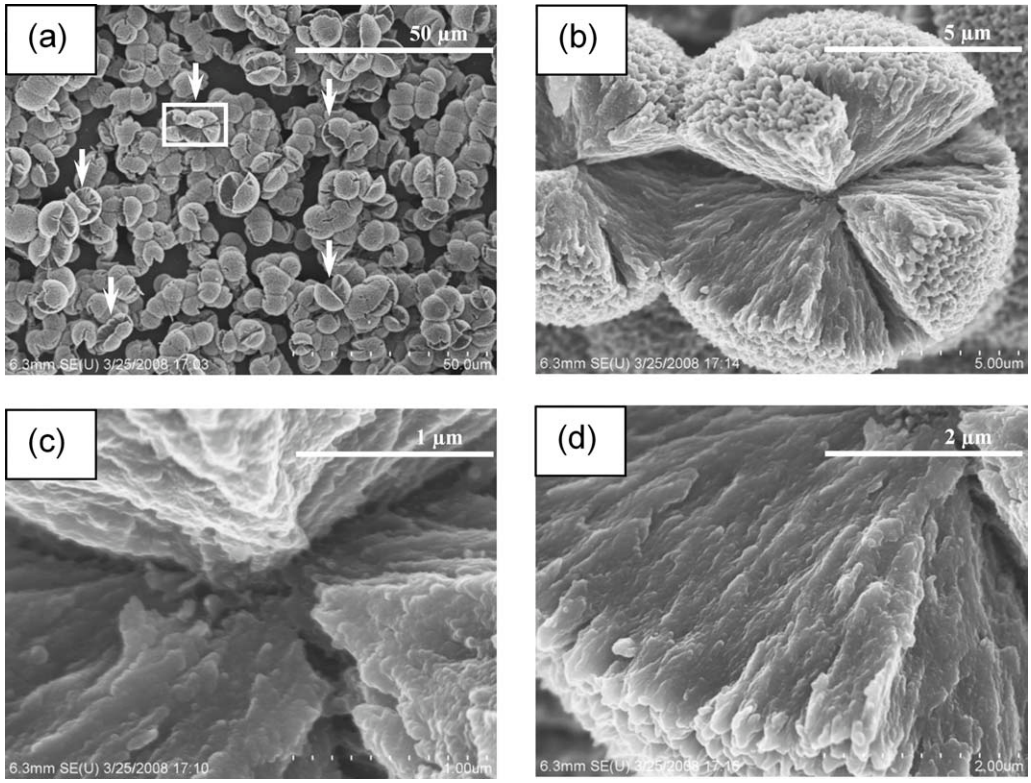

Figure 4 SEM images for the crystallized BAPC thin film right above the contact line (a) incomplete spherulites, (b) enlarged view of open-structured three-dimensional spherulites, (c) center of the spherulite, and (d) enlarged view of lamellar structures radiating from the spherulitic center.

spherulite transformation and similar spherulitic structures along the thickness direction of the film suggest that the concentration gradient inside the film along the thickness direction is negligible in the film since the major concentration gradient is in the vertical direction, not in the direction of film thickness. Also, it is notable that these spherulite particles are mostly split, showing the interior morphology.

The morphologies of spherulites shown in Figure 3(h) are further analyzed using Hitachi SU-70 SEM with a relatively low operating voltage (e.g., 5 kv). The image in Figure 4(a) clearly shows that the amorphous BAPC film has been completely converted to spherical or three-dimensional spherulites. Most of the spherulites were also connected to neighboring spherulites with large voids between them. A great number of the spherulites showed sharp edges or crack-like structures as indicated by arrows in Figure 4(a). The highly magnified image of joined spherulites with crack-like features is shown in Figure 4(b). The crack seemed to reach all the way to the nucleus of the spherulite [Fig. 4(c,d)], indicating that SINC did not occur homogenously and uniformly to yield ideal spherical particles. The crack-like features in the spherulites are likely to be formed by anisotropic crystal growth in discrete bundles due to the limited material supply during the crystallization in the thin film. The opened, unfilled area of the spherulites revealed the internal structures of spherulites where lamellar structure radiated from the center of the spherulite. In literature, spherulites with such crack-like features have not been reported in a conventional process of SINC. Surprisingly, there are only few reports that have experimentally showed open-structured spherulites under other crystallization conditions in the literature. The pine-shaped (or dendrite-spherulite) substructures were reported in the cross section of spherulites of poly(ethylene terephthalate) (PET) prepared under high pressure.[29] The formation of such substructures was speculated to be caused by the secondary nucleation of crystal grains at the crystal growth front in the spherulites.[30] In this study, the pine-shaped substructure was not observed in the open-structured BAPC spherulites, suggesting that there was no secondary nucleation at the crystal growth front. Intermittent branches and other types of substructures were not able to be distinguished clearly from the SEM images as well.

As a comparison, Figure 5 shows the SEM images of crystallized BAPC spherulites formed in the region below the liquid–air contact line (i.e., immersed in a liquid acetone). Direct contact between the BAPC film and acetone caused rapid crystallization from more nucleation sites, resulting in smaller (3–5 μm) and coarse spherulitic lamellar

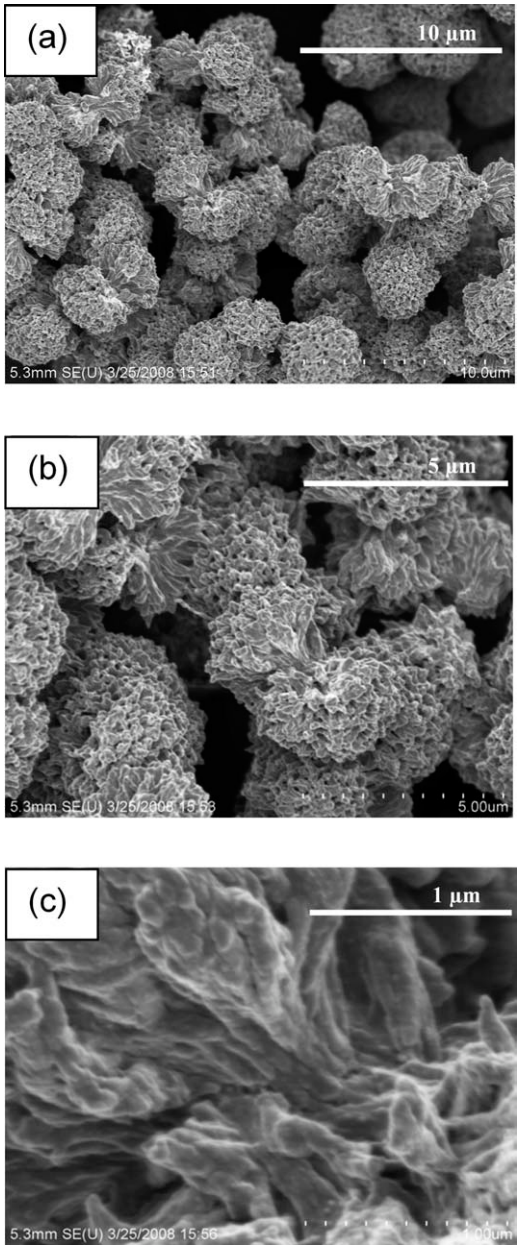

Figure 5 SEM images for the crystallized BAPC thin film below the contact line (a) spherulites, (b) enlarged view of dumbbell-structured spherulites, and (c) center of the dumbbell-shaped spherulites.

structures shown in Figure 5(a) as compared with relatively larger (5–10 μm) and finer spherulitic structures developed right above the contact line. In Figure 5(b), the dumbbell-structured morphology shows discrete bundles which are usually observed in an intermediate stage of spherulitic growth from a nucleus to a fully developed three-dimensional spherulite. However, the open-structured spherulites with sharp edges observed above the contact line were not found below the contact line. Figure 5(c) is an enlarged view of the center of the dumbbell-like spherulites shown in Figure 5(b), revealing rough crystalline structures compared with Figure 4(c) where the crystallization occurred under a more controlled manner. These morphological features are in sharp contrast with the finer lamellar structures formed right above the contact line, suggesting that the faster crystallization below the contact line is likely to have occurred at the higher number of nucleation sites, resulting in a higher number of smaller spherulites. This also suggests that the controlled SINC process in a thin film allows us to access a wider range of morphological patterns and features which were not readily obtained from a conventional SINC.

Figure 6 shows the AFM height images of different morphologies above the contact line. In Figure 6(a), the AFM image of the region above the diffusion front exhibits no sign of crystallization. The images from the regions between the diffusion front and the contact line captures more detailed processes of the crystallization occurring on a thin film during SINC process. In Figure 6(b), it is seen that the lamellae grew radially from the potential nucleation site (marked with an arrow), but branching was not observed along the lamellar structures. As the acetone concentration increases, Figure 6(c) exhibits intermittent branching (marked with an arrow) and splaying (marked with a box) which is a hallmark of lamella growth to form large spherulites. This morphology is very similar to the lamella formed during the crystallization of a very thin poly(bisphenol A hexane ether) film.[31] Right above the contact line, the height image of fully grown spherulites shown in Figure 6(d) indicates fine structures of thin leaf-like crystal growth front started from the center of the spherulite.

Although many studies have been reported on the morphology of three-dimensional spherulites,[12–16,32–35] this study shows that spherulites formed from thin film can develop to two distinct morphologies depending on the locations of their growth; whether they grew above or below the air–liquid contact line. Below the air–liquid contact line, the dumbbell shape morphology was observed. This morphology is formed by unidirectional growth at the nuclei and low angle branching, resulting in the formation of two "eyes" as shown in Figure 5(a). The spherulites formed above the air–liquid contact line were more spherical morphologies, indicating that lamellae grew in a multidirectional way from the center uniformly. We speculate that the different nucleation rate and crystallization rate above and below the contact line is the major reason for different morphologies. In addition, spherulites formed above the contact line showed three-dimensional open-structured spherulites that are not often observed even under other crystallization conditions.[29,36] Although the formation mechanism of

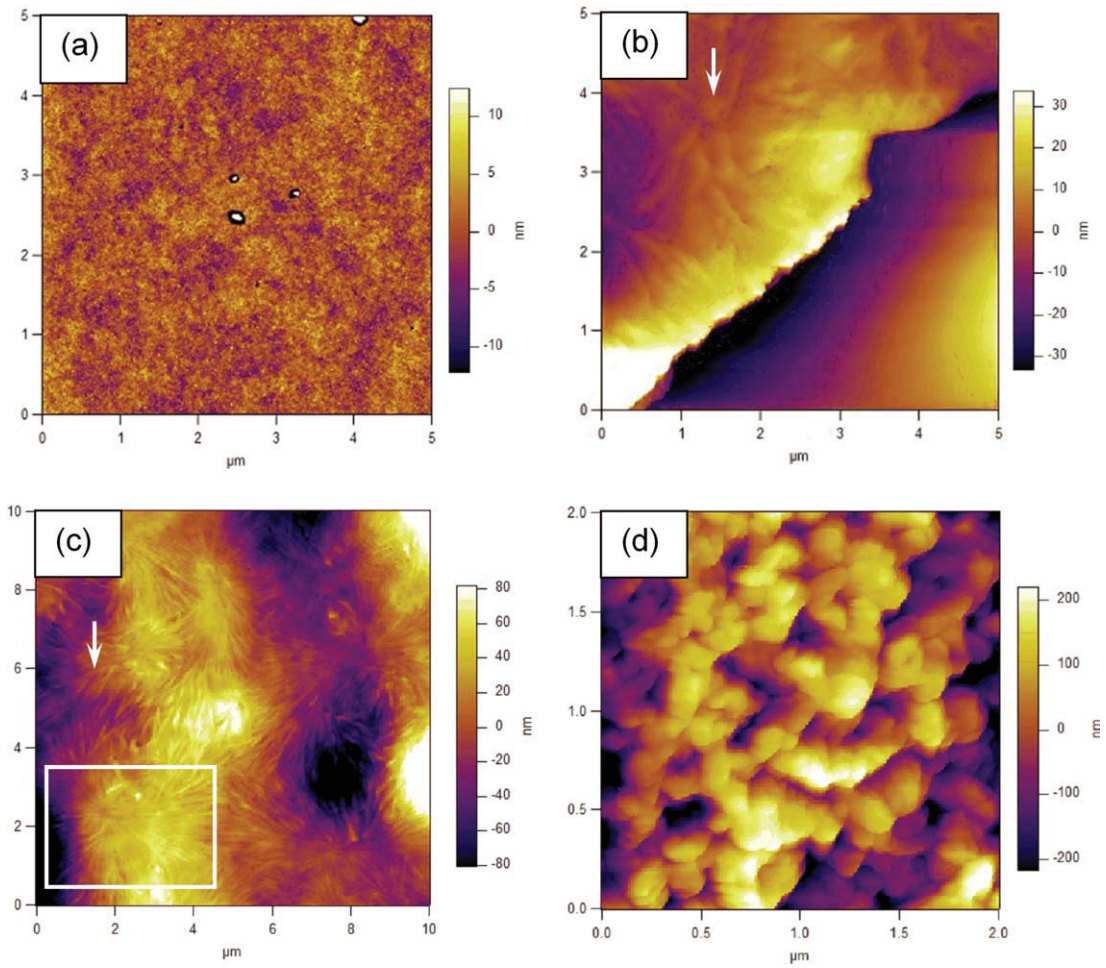

Figure 6 AFM height images of morphology patterns above the contact line. The approximate distances from the contact line were (a) 20 mm, (b) 9 mm, (c) 8 mm, and (d) 0.1 mm. [Color figure can be viewed in the online issue, which is available at wileyonlinelibrary.com.]

open-structured spherulites is not fully understood, the incomplete spherulites with unfilled space are likely to be caused by insufficient amount of polymer available, which hindered the continuous growth of the spherulites.

CONCLUSIONS

In this article, we have reported the transitions of morphological patterns of a crystallizing BAPC film when it was partially immersed in a liquid acetone bath. The diffusion of liquid acetone along the plane in a 5.5-μm film occurred much faster than that in the bulk BAPC polymer, probably due to micrometer-sized diffusion channels such as cracks and cavities that developed in the film when exposed to acetone. The concentration gradient in a thin film created by this diffusion process caused a formation of a wide variety of morphologies that were not readily observed in a conventional SINC. It should be noted that as compared with the concentration gradient perpendicular to the direction of film thickness, the concentration gradient along the film thickness direction is negligible in a thin film. However, the film thickness affects the formation of cracks, voids that may further affect penetration depth and morphology. Surface images obtained by AFM confirmed that the BAPC spherulite grew radially from the nucleation site and then branched intermittently to form the spherulitic structure. Both SEM and AFM results indicate that the growth of these spherulites occurs in discrete bundles then merge and form into a complete three-dimensional spherulites. The method presented in this work can also be used to investigate the internal structures of spherulites formed under different acetone concentrations and thereby better understand the SINC mechanism in thin polymer films.

References

1. Falkai, B. V.; Rellensmann, W. Makromol Chem 1965, 88, 38.
2. Siegmann, A.; Geil, P. H. J Macromol Sci Part B: Phys 1970, 4, 239.
3. Gallez, F.; Legras, R.; Mercier, J. P. J Polym Sci Part B: Polym Phys 1976, 14, 1367.

4. Bailly, C. H.; Daumerie, M.; Legras, R.; Mercier, J. P. J Polym Sci Part B: Polym Phys 1985, 23, 751.
5. Mercier, J. P.; Groeninckx, C.; Lesne, M. J Polym Sci Polym Symp 2059 1967, 16.
6. Fan, Z.; Shu, C.; Yu, Y.; Zaporojtchenko, V.; Faupel, F. Polym Eng Sci 2006 46, 729.
7. Beckman, E.; Porter, R. S. J Polym Sci Part B: Polym Phys 1987, 25, 1511.
8. Falkai, B. V.; Hinrichsen, G. J Polym Sci Part C: Symp 1977, 58, 225.
9. Djurner, K.; Manson, J.-A.; Rigdahl, M. J Polym Sci Polym Lett Ed 1978, 16, 419.
10. Harron, H. R.; Pritchard, R. G.; Cope, B. C.; Goddard, D. T. J Polym Sci Part B: Polym Phys 1996, 34, 173.
11. McNulty, B. J Polymer 1968, 9, 41.
12. Fryer, R. E. J. J Appl Polym Sci 1974, 18, 2261.
13. Wilkes, G. L.; Parlapiano, J. Polym Prep 1976, 17, 937.
14. Mochizuki, H.; Mizokuro, T.; Tanigaki, N.; Ueno, I.; Hiraga, T. J Polym Sci Part B: Polym Phys 2005, 43, 2307.
15. Zhao, N.; Weng, L.; Zhang, X.; Xie, Q.; Zhang, X.; Xu, J. ChemPhysChem 2006, 7, 824.
16. Ye, Y.; Choi, K. Y. Macromol Mater Eng 2009, 294, 847.
17. Woo, B. G.; Choi, K. Y.; Song, K. H.; Lee, S. H. J Appl Polym Sci 2001, 80, 1253.
18. Kambour, R. P.; Karasz, F. E.; Daane, J. H. J Polym Sci Part A-2: Polym Phys 1966, 4, 327.
19. Alfrey, T., Jr.; Gurnee, E. F.; Lloyd, W. G. J Polym Sci Part C: Polym Symp 1966, 12, 249.
20. Miller, G. W.; Visser, S. A. D.; Morecroft, A. S. Polym Eng Sci 1971, 11, 73.
21. Turska, T.; Benecki, W. J Appl Polym Sci 1979, 23, 3489.
22. Ware, R. A.; Tirtowidjojo, S.; Cohen, C. J Appl Polym Sci 1981, 26, 2975.
23. Liu, C. K.; Hu, C. T.; Lee, S. Polym Eng Sci 2005, 45, 687.
24. Crank, J. The Mathematics of Diffusion, 2nd Ed. Oxford University Press: Oxford, 1975.
25. Wang, T. T.; Kwei, T. I. J Polym Sci Part A-2 1969, 7, 2019.
26. Vrentas, J. S.; Duda, J. L. J Polym Sci Part B: Polym Phys 1977, 15, 417.
27. Ouyang, H.; Wu, M. T. J Appl Phys 2004, 96, 7066.
28. Kitagawa, M. J Polym Sci Part B: Polym Phys 1979, 1974, 12.
29. Li, L.; Rui, H.; Lu, A.; Fan, W.; Hong, S.; Fu, Q. J Cryst Growth 2000, 216, 538.
30. Gránásy, L.; Pusztai, T.; Tegze, G.; Warren, J. A.; Douglas, J. F. Phys Rev E 72 2005, 29, 1.
31. Wang, Y.; Chan, C.-M.; Ng, K.-M.; Li, L. Macromolecules 2008, 41, 2548.
32. Desaif, A. B.; Wilkes, G. L. J Polym Sci Part C: Polym Symp 1974, 46, 291.
33. Makarewicz, P. J.; Wilkes, G. L. J Appl Polym Sci 1979, 23, 1619.
34. Durning, C. J.; Rebenfeld, L.; Russel, W. B.; Weigmann, H. D. J Polym Sci Part B: Polym Phys 1986, 24, 1341.
35. Cheng, L.-P.; Young, T.-H.; Chuang, W.-Y.; Chen, L.-Y.; Chen, L.-W. Polymer 2001, 42, 443.
36. Lu, J.; Oh, I.-K.; Huang, R.; Wang, X.-L. Adv Mater Res 2007, 26, 1275.